J Nanopart Res (2018) 20: 204
https://doi.org/10.1007/s11051-018-4291-6

RESEARCH PAPER

A novel, chelator-free method for ^{64}Cu labeling of dendrimers

Xiaoping Xu · Yi Li · Tianye Cao · Jingyi Cheng · Yingjian Zhang

Received: 9 May 2018 / Accepted: 29 June 2018 / Published online: 24 July 2018

Abstract Nanoparticles (NPs) have been widely used in biomedical research, but the difficulty in determining their in vivo characteristics limits their clinical translation. So far, positron emission tomography (PET), which requires that the NPs are labeled with an appropriate positron nuclide, appears to be the most likely solution to this problem. ^{64}Cu is the most frequently used positron emitter in NP research and ^{64}Cu radiolabeling using chelators is the most commonly used strategy, although this method has some shortcomings in practice. In the present study, we directly integrated ^{64}Cu into the internal cavities of generation 5 polyamidoamine (G5 PAMAM), a commercially available NP, without the need for chelators. The labeling time, pH level, temperature, and amount of precursor were systematically varied to determine the optimum labeling conditions. Preliminary biological evaluation in mice revealed that the ^{64}Cu direct labeling method was feasible for the preparation of labeled PAMAM for in vivo studies. This study introduced a novel idea for ^{64}Cu labeling of dendrimers (and other NPs with a similar structure) and should facilitate the application of NPs in biomedical studies.

Keywords Nanoparticles · PAMAM dendrimer · PET imaging · ^{64}Cu radiolabeling · Biomedicine

X. Xu · Y. Li · T. Cao · J. Cheng · Y. Zhang (✉)
Department of Nuclear Medicine, Fudan University Shanghai Cancer Center, Shanghai 200032, China
e-mail: yjzhang111@aliyun.com

X. Xu · Y. Li · T. Cao · J. Cheng · Y. Zhang
Department of Oncology, Shanghai Medical College, Fudan University, Shanghai 200032, China

X. Xu · Y. Li · T. Cao · J. Cheng · Y. Zhang
Center for Biomedical Imaging, Fudan University, Shanghai 200032, China

X. Xu · Y. Li · T. Cao · J. Cheng · Y. Zhang
Shanghai Engineering Research Center of Molecular Imaging Probes, Shanghai 200032, China

J. Cheng · Y. Zhang
Shanghai Proton and Heavy Ion Center, Fudan University Shanghai Cancer Center, Shanghai 200032, China

Introduction

Nanoparticles (NPs) have been widely used in biomedical research, including drug delivery and molecular imaging (Shi et al. 2016; Pelaz et al. 2017; Bose et al. 2014). Highly flexible and modified NPs enable tunability in vivo pharmacokinetics to improve delivery efficiency and nonspecific binding can be reduced by varying size, charge, and surface modifications (Kinnear et al. 2017). For a better clinical translation, the in vivo characteristics of nanoparticles must be clear. Reliable and quantitative evaluation of nanoparticles in vivo is, however, still a big challenge because a direct study of NPs in tissues is arduous and cannot be extrapolated to human clinical studies (Wang et al. 2012). In order to overcome this obstacle, various imaging approaches have been used to assess the in vivo characteristics of NPs. Among these, positron emission tomography

(PET) is the most commonly used imaging method because of its high sensitivity (picomolar level), unlimited tissue penetration, and accurate quantitative results (Cheng et al. 2012; Smith and Gambhir 2017). PET imaging depends on a pair of photons emitted by positron nuclides that emanate from the collision site in opposite directions. NPs thus need to be labeled with a positron nuclide when PET imaging is used to study their in vivo characteristics. Although many positron nuclides are available, there is a limited choice of positron nuclides that are suitable for labeling NPs because a relatively long half-life and simple labeling method are required (Liu and Welch 2012).

Cu-64, which has an appropriate half-life ($T_{1/2}$ = 12.7 h) and straightforward labeling chemistry, has been frequently used as the positron nuclide in NP applications (Anderson and Ferdani 2009). A wide variety of chelators that can easily link to the surface of NPs are currently used for conjugating ^{64}Cu to NPs (De Silva et al. 2012), but all of these coordinative chelators have some shortcomings. For instance, one of the most frequently used macrocyclic chelators, 1,4,7,10-tetraazacyclododecane-1,4,7,10-tetraacetic acid (DOTA), is unsatisfactory in vivo stability, which may result in the trans-chelation of ^{64}Cu to proteins and high uptake in non-targeted organs, thus affecting the final quantitative results (Boswell et al. 2004; Bass et al. 2000). Modified cross-bridged macrocyclic chelators show improved kinetic stability compared with DOTA, but these ligands generally require harsh conditions, which are unsuitable for some biologically active target molecules, to coordinate with ^{64}Cu (Wadas and Anderson 2007). Chelators that are linked to NPs through a covalent bond may also influence the in vivo pharmacokinetics of the NPs, which must counteract the conjugation of the chelators. Methods that allow direct ^{64}Cu labeling of NPs, without chelators, are likely to overcome these shortcomings and the characteristics of NPs allow chelator-free labeling. There has been extensive research on NP-metal conjugation, which can be extrapolated to the combination of NPs and ^{64}Cu (Hong et al. 2017; Wang et al. 2017; Gawande et al. 2016).

Polyamidoamine (PAMAM) is a unique globular NP with a highly branched structure, which produces a large number of interior cavities and terminal groups (Taghavi Pourianazar et al. 2014). The tree-like structure produces internal cavities with different sizes, which can be used as templates to synthesize PAMAM-entrapped metal colloids. A wide range of metal particles, including Cu, Ag, Au, Pt, Pd, and Rh have been trapped within PAMAM (Balogh et al. 1999; Crooks et al. 2001). A Cu-PAMAM nanocomposite, in which the Cu^{2+} ions were conjugated with tertiary amines inside PAMAM, was first reported by Zhao et al. (1998). Since then, research into Cu-dendrimer complexes has flourished and different synthetic methods have been developed to produce nanoscale Cu-dendrimer conjugates of various sizes (Zhao and Li 2011; Caminade et al. 2015; Nemanashi and Meijboom 2013). Nevertheless, most of this research was focused on catalytic applications and little attention was devoted to biomedicine (Ficker et al. 2015; Maity et al. 2013). An earlier study by our group first introduced the application of Cu-PAMAM in biomedical imaging. Cu^{2+} ions were encapsulated in folic acid-modified PAMAM and synchrotron X-ray fluorescence was used to image the distribution of Cu-PAMAM in cells (Zhang et al. 2013). Although synchrotron X-ray fluorescence cannot be used for imaging in live animals because of its high energy, this earlier study provided the feasibility for using PAMAM-encapsulated ^{64}Cu in PET imaging. In the present study, we first developed a method for preparing PAMAM-encapsulated ^{64}Cu ions and then carried out a preliminary evaluation of the biodistribution of the ^{64}Cu-PAMAM nanocomposite to provide the basis for future applications in PET imaging and biomedicine.

Materials and methods

G5 PAMAM dendrimers were purchased from Dendritech Inc. (Midland, MI, USA). Maltose, sodium hydroxide, ethylenediaminetetraacetic acid, borax, boric acid, borane-pyridine complex, and deuteroxide were obtained from Sinopharm Chemical Reagent Co., Ltd. (Shanghai, China). Acetonitrile (ACN) and trifluoroacetic acid (TFA) were purchased from J&K Science Co., Ltd. (Shanghai, China). ^{64}Ni powder (99.9%) was purchased from Isotope industrial International Co., Ltd. (Shenzhen, Guangdong, China). Ultra pure nitric acid and hydrochloric acid were purchased from Merck (Darmstadt, Hesse, German). Dialysis membranes (molecular weight cut off, MWCO 14,000 Da) were obtained from Union Carbide

Corporation (Houston, TX, USA). Female Kunming normal mice were obtained from the Shanghai Laboratory Animal Center, Chinese Academy of Sciences.

The radiopharmaceutical was analyzed using an Agilent 1200 HPLC system (Agilent Technologies, Santa Clara, CA, USA), equipped with a Raytest GABI flow-through γ-detector (Elysia & Raytest, Straubenhardt, Baden, Germany). A Phenomenex (Torrance, CA, USA) Jupiter C5 silica-based column (250 × 4.6 mm, 5 μm) was used for the analysis. The mobile phase was a mixture of ACN and water containing 0.14 wt% TFA. Linear gradient elution was used, beginning with 90% water and reaching 50% water after 30 min. Analyses were carried out at room temperature, with a flow rate of 1 mL/min.

Preparation of G5 PAMAM-maltose

A borane-pyridine complex (55 μL) was added dropwise to a solution of G5 PAMAM (200 mg) and maltose (190 mg) in borate buffer (0.1 M, pH = 9, 10 mL) and the mixture was then stirred at 50 °C for 7 days (Scheme 1). The product was purified by dialysis against phosphate-buffered saline (PBS, pH = 7.4) and deionized water, using dialysis membranes with a molecular weight cut off of 14,000 Da, and then lyophilized. The final conjugate was characterized by ^{1}H NMR using an ECZ 400-MHz spectrometer (JEOL, Tokyo, Japan), with D_2O as the solvent. The morphology of G5 PAMAM-maltose (G5-Mal) was further determined by a transmission electron microscope (TEM, FEI Tecnai G2 F20 S-TWIN, USA).

Preparation of ^{64}Cu

No carrier-added ^{64}Cu was produced using the ^{64}Ni (p, n) ^{64}Cu nuclear reaction. The enriched ^{64}Ni powders were electroplated onto a gold target using an ALCEO EDL module (Comercer S.p.A, Castel Bolognese, RA, Italy). The ^{64}Ni plating target was then bombarded with an 11-MeV proton beam of 30-μA intensity, using an Eclipse HP cyclotron (Siemens AG, Munich, Germany). After irradiation, the target was transferred to the EDL module and dissolved in 6 M HCl at 90 °C. The resulting solution was purified using the ADDEO PRF module to recover enriched ^{64}Ni and collect the final product, $^{64}CuCl_2$, which was identified using an HPGe detector (GEM-C5060P4, Ortec, Oak Ridge, TN, USA).

Radiolabeling G5-Mal with $^{64}CuCl_2$

Mixtures of $^{64}CuCl_2$ solution (10 μL) and aqueous G5-Mal solution (90 μL) were incubated for various times at different temperatures. The concentration of G5-Mal and the pH level of the reaction mixture were also varied to determine the optimal radiolabeling conditions (Scheme 1). The radiolabeled yield was determined using HPLC.

In vitro stability

The in vitro stability of G5-Mal-^{64}Cu was evaluated by incubation in PBS (0.1 M, pH = 7.4) and in 20 mM ethylenediaminetetraacetic acid (EDTA) solution (> 1000 M equivalents) over the radiolabeled compound up to 12 h. G5-Mal-^{64}Cu was further assessed in the fresh mouse plasma where the in vivo environment was mimicked. After precipitation of plasma proteins with ACN, degradation of the ^{64}Cu was assessed by HPLC.

Biodistribution study in mice

The animal study was approved by Fudan University Laboratory Animal Ethics Committee. G5-Mal-^{64}Cu (0.37 MBq) was injected as a slow intravenous bolus into the tail vein of female Kunming mouse ($n = 21$). The mice were divided into seven groups, which were sacrificed 0.5, 1, 2, 4, 6, 12, and 24 h after injection. Blood and tissue samples were collected and weighed, and radioactivity was measured using a γ-counter. All data were corrected for background radioactivity and radioactive decay. The amount of radioactivity was expressed as the percentage of injected dose per gram of tissue or blood (ID%/g). Measured tissues were heart, liver, spleen, lung, kidney, stomach, intestine, skin, muscle, bone, and brain.

Results

Synthesis and characterization of G5-Mal

Maltose was conjugated onto surface amino groups of G5 PAMAM by reductive amination of monodendrons and dendrimers with different excesses of oligosaccharide, as previously described (Gajbhiye et al. 2013). The desired maltose-modified PAMAM dendrimer was successfully synthesized and isolated by dialysis in PBS and deionized water to remove excess maltose. The

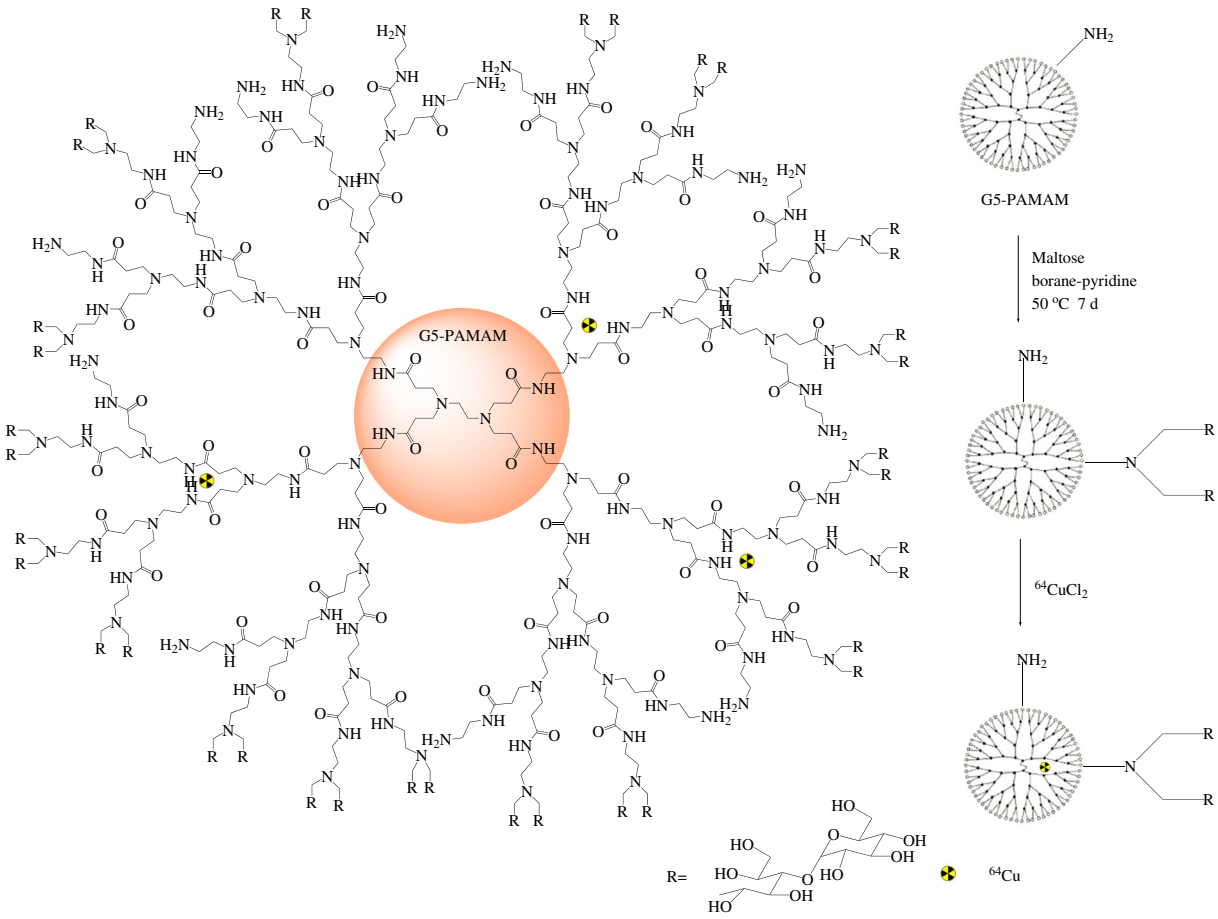

Scheme 1 Synthesis of G5-Mal-^{64}Cu

overall synthetic yield was ~ 70%. The number of maltose residues coupled to G5 PAMAM surface amino groups was calculated using ^{1}H NMR spectroscopy. The ^{1}H NMR of G5-Mal showed two characteristic peaks (Fig. 1a). The peak at 2.42 ppm corresponded to methylene protons of –CH_2C(O)– groups in the PAMAM dendrimer and the peak at ~ 5.10 ppm corresponded to specific anomeric CH– group protons of maltose (Klajnert et al. 2008). The integration ratio of these two types of proton signals in G5-Mal suggested that an average of 88 maltose residues were coupled to each G5 PAMAM (G5-Mal_{88}). The characterization of G5-Mal_{88} with TEM was illustrated in Fig. 1b.

Preparation of ^{64}Cu

^{64}Cu was eluted from the ion exchange resin in the form of $^{64}CuCl_2$ using 0.5 M HCl. After 30-min irradiation and 2-h purification, 370 MBq of $^{64}CuCl_2$ was obtained. The radionuclide purity was determined using an HPGe detector and the γ spectrum is shown in Fig. 2. In addition to the characteristic peak of the positron nuclide at 511 keV, there was one other peak at 1346 keV, which was attributed to ^{64}Cu. These results indicated that the acquired ^{64}Cu possessed high radionuclide purity.

Radiolabeling G5-Mal_{88} with $^{64}CuCl_2$

The labeling yields obtained using different reaction times, pH values, temperatures, and quantities of G5-Mal_{88} were measured by HPLC to determine the optimum conditions. As shown in Fig. 3, good labeling was achieved with a pH value of 7, a reaction temperature of 25 °C, and 1 mg/mL of G5-Mal_{88}. High labeling yields were obtained after 15 min. The HPLC characterization of the starting materials and final product is shown in Fig. 4. The retention time of G5-Mal_{88}-^{64}Cu

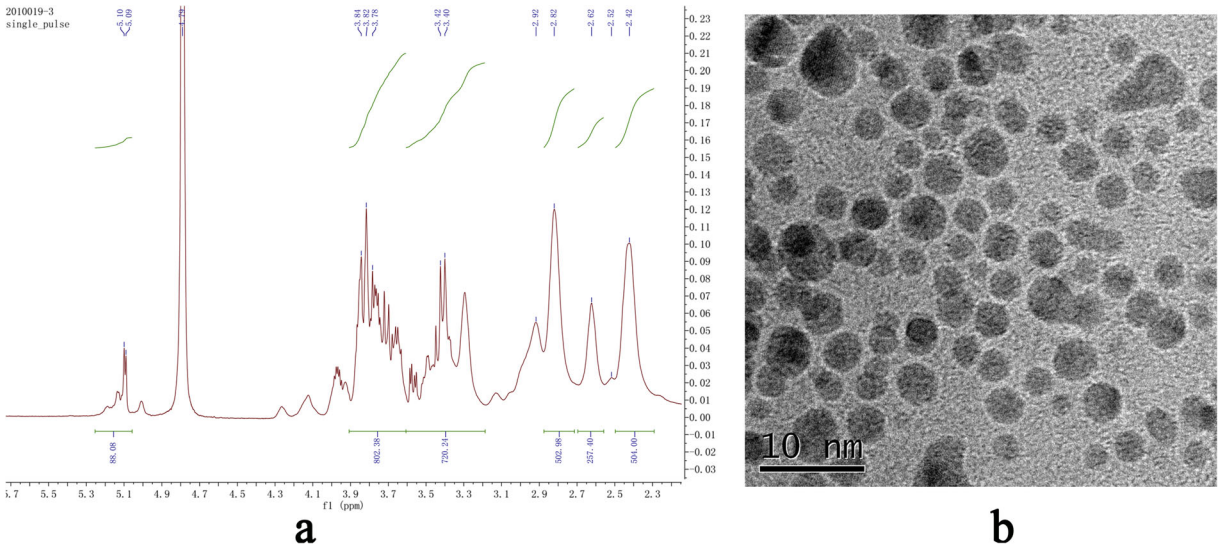

Fig. 1 The characterization of G5-Mal_{88}. **a** ^{1}H NMR spectrum. **b** TEM image

(11.298 min) was similar to that of the labeling precursor, G5-Mal (10.579 min), whereas the retention time of $^{64}CuCl_2$ was 4.353 min.

In vitro stability

The stability of G5-Mal_{88}-^{64}Cu in PBS, EDTA, and mouse plasma is shown in Fig. 5. G5-Mal_{88}-^{64}Cu was very stable in PBS and retained 95% radioactivity in the form of G5-Mal-^{64}Cu after 12-h incubation. The EDTA challenge experiment revealed that G5-Mal_{88}-^{64}Cu remained stable and approximate 12.5% radioactive decomposition was observed after 12-h incubation. G5-Mal_{88}-^{64}Cu was less stable in mouse plasma, where some radioactive decomposition (~ 15%) was observed.

Biodistribution of G5-Mal-^{64}Cu

The biodistribution of G5-Mal_{88}-^{64}Cu in normal mice is displayed in Fig. 6. G5-Mal_{88}-^{64}Cu accumulated mostly

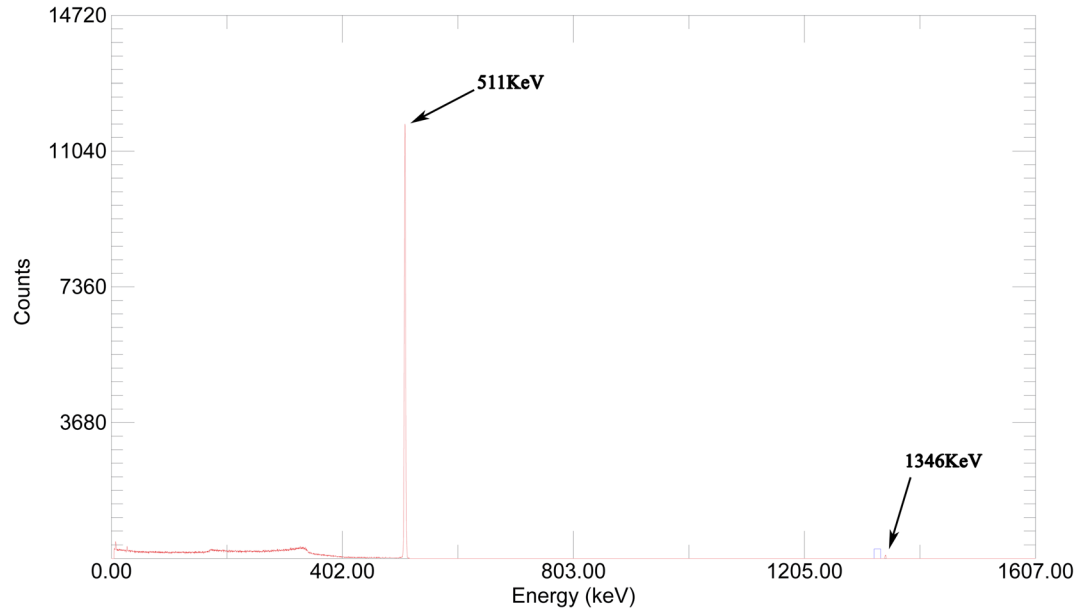

Fig. 2 γ-ray energy spectrum of $^{64}CuCl_2$ obtained using HPGe

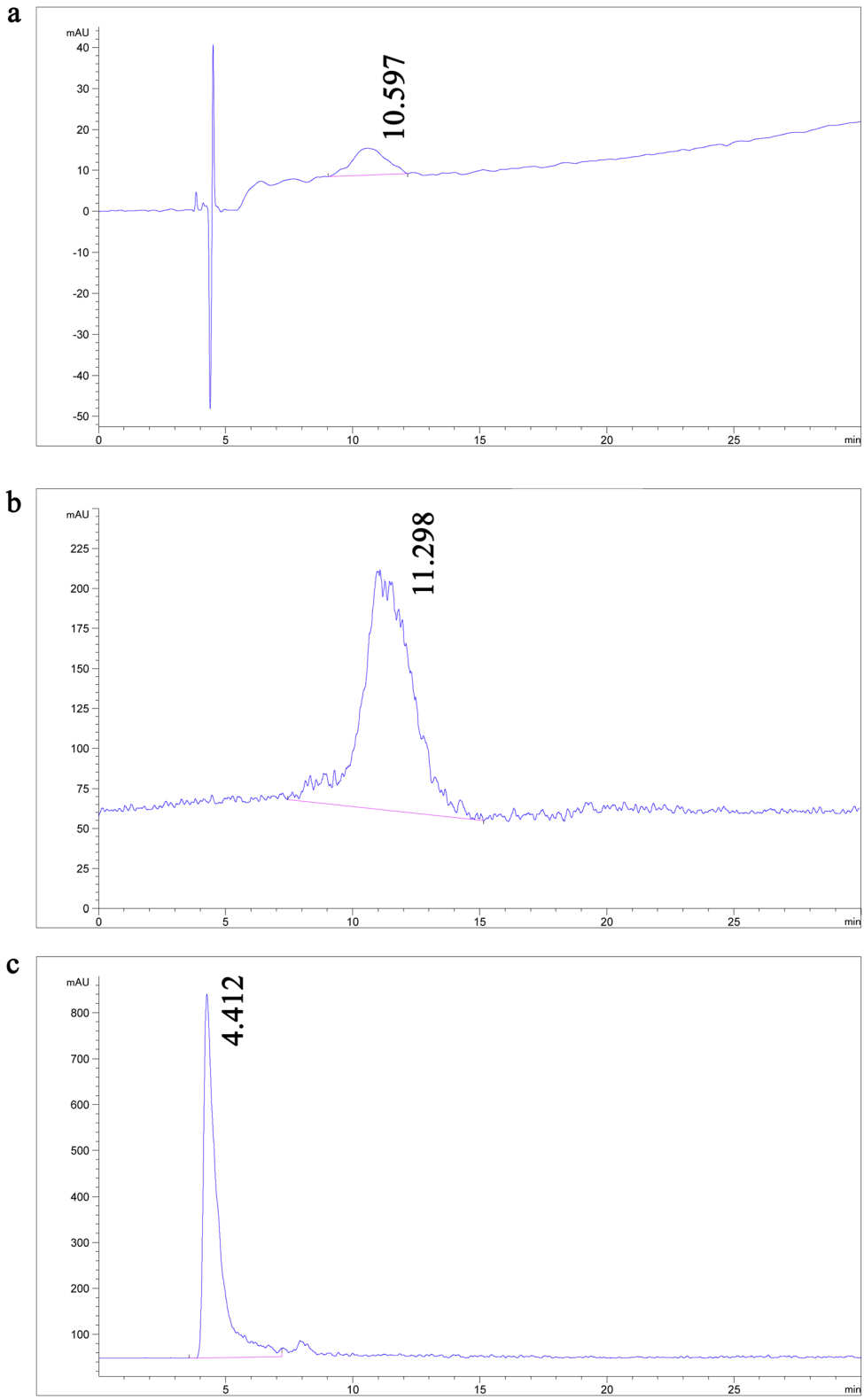

Fig. 3 HPLC characterization. **a** UV spectrum of G5-Mal_{88}. **b** Radioactive spectrum of G5-Mal_{88}-^{64}Cu. **c** Radioactive spectrum of $^{64}CuCl_2$

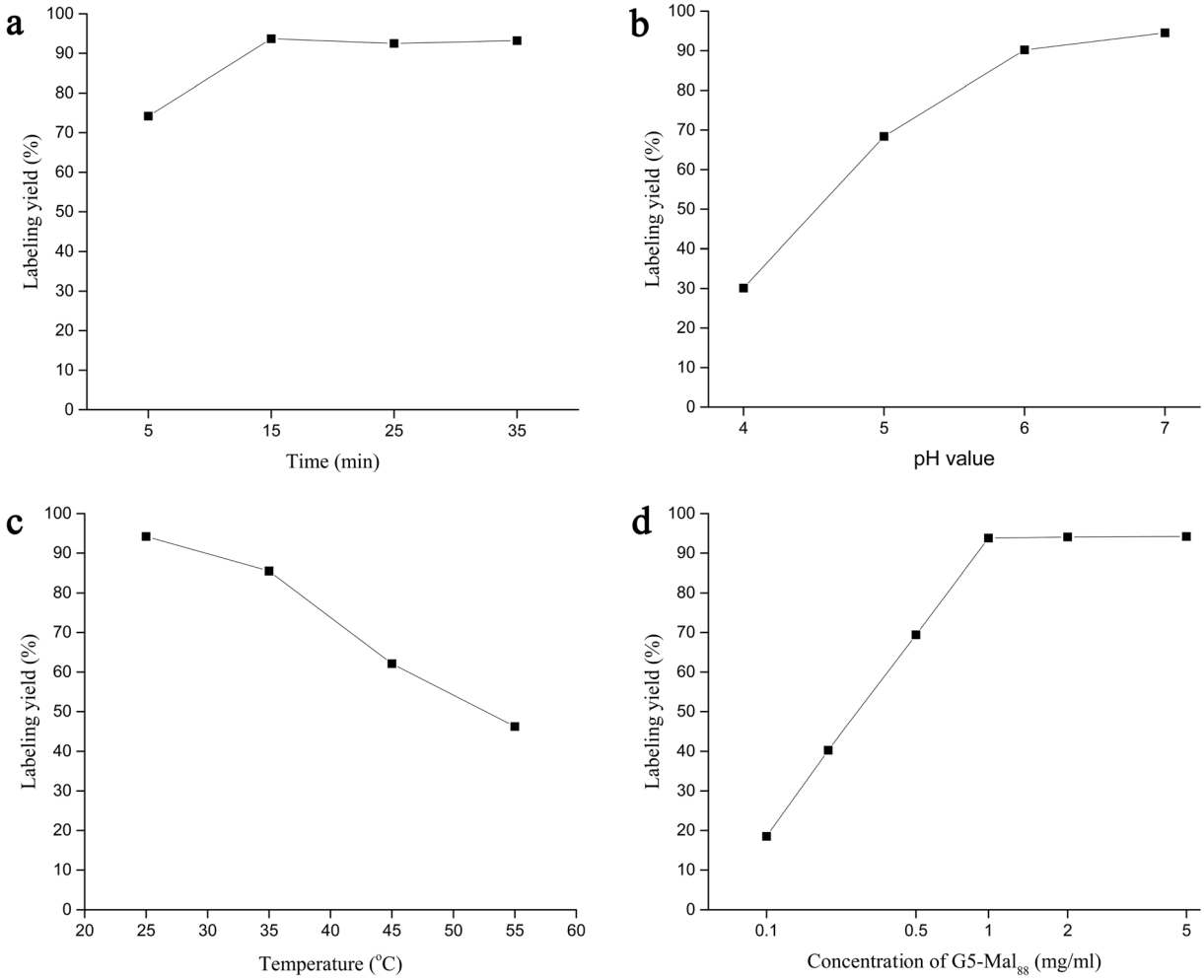

Fig. 4 Yields of ^{64}Cu labeling G5-Mal$_{88}$ obtained under different conditions. **a** Correlation between labeling yield and reaction time. **b** Correlation between labeling yield and pH. **c** Correlation between labeling yield and temperature. **d** Correlation between labeling yield and concentration of G5-Mal$_{88}$

in the liver and reached a peak at 1 h after injection (45.75 ± 8.60 ID%/g). Then, the accumulation reduced with the increase of time and reached 20.27 ± 2.57 ID%/g at 24 h after injection. The spleen was the second highest radioactive concentrated organ. The radioactivity of spleen peaked at 0.5 h after injection (38.72 ± 8.81 ID%/g) and reduced to 5.43 ± 1.24 ID%/g at 24 h after injection. G5-Mal$_{88}$-^{64}Cu was rapidly cleared from blood and blood radioactivity was very low 6 h after injection (ID%/g = 0.68 ± 0.21). The kidney was the third major organ with high radioactivity, indicating that G5-Mal$_{88}$-^{64}Cu was likely to be excreted partly through the kidney. The radioactivity in kidney maintained a high level within 6 h after injection, from 7.05 ± 1.72 ID%/g to 6.13 ± 1.72 ID%/g. After 24 h of injection, the accumulation of G5-Mal$_{88}$-^{64}Cu remained 2.33 ± 0.49 ID%/g. The remaining tissues showed comparatively low radioactivity, which decreased over time in all tissues.

Discussion

Nanomaterials have been studied for almost 40 years and have achieved great success in many fields (Murty et al. 2013; Tiwari et al. 2012). Nevertheless, the successful translation of NPs into the clinic remains lower than in other areas, which has been mostly attributed to the intricate internal environment of the human body. It is extremely difficult to evaluate the in vivo

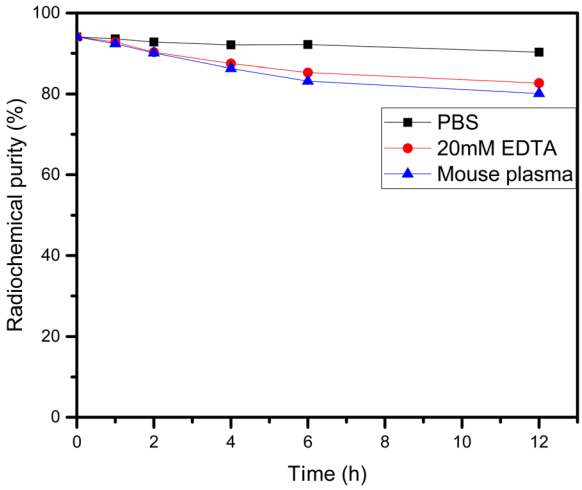

Fig. 5 Stability of G5-Mal$_{88}$-^{64}Cu in PBS, 20 mM EDTA, and mouse plasma

characteristics of NPs without using anatomical experiments in animals, and such experiments, which are destructive and need a large number of samples, are very costly and time-consuming (Wang et al. 2012). Moreover, the destructive experimental methods used on animals cannot be extended to humans, and individual differences in large samples may lead to false conclusions. Nondestructive imaging technology can be used to overcome the problems associated with the use of NPs in biomedical research (Chen, 2011; Rosenblum et al. 2010). PET imaging, especially, has attracted much attention because PET is able to quantitatively detect any target tissue in vivo. Commercially available matched human PET/CT and animal PET/CT have facilitated the progress of PET in translational research on

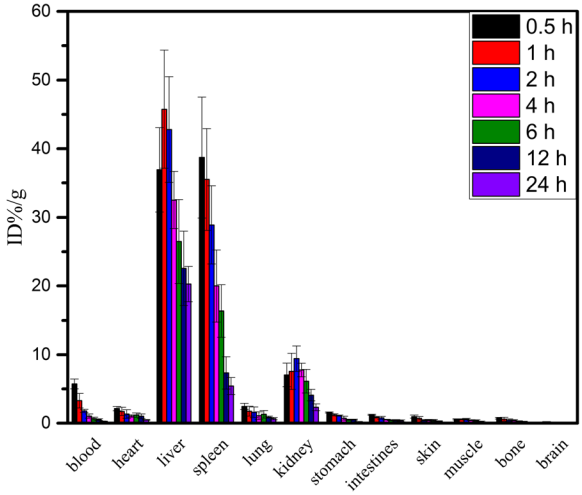

Fig. 6 Biodistribution of G5-Mal$_{88}$-^{64}Cu in normal mice ($n = 3$)

NPs. Over the past decades, growth in the applications of NPs in biomedicine using PET imaging has contributed to drug discovery and led to numerous clinical trials (Colombo et al. 2017; Heidel and Davis 2011; Padmanabhan et al. 2016; Xing et al., 2014). All of these achievements are based on the premise that the NPs could be labeled by positron nuclides, which is a prerequisite in PET imaging.

For large NPs with a long circulation time in vivo, the specific positron isotope must be carefully considered to generate an optimal outcome. Because of its favorable radioactive properties and mature labeling chemistry, ^{64}Cu is the most widely used positron nuclide for NPs in PET imaging. So far, ^{64}Cu has been mainly attached to NPs using bifunctional chelating agents (Wadas et al., 2010), which have been demonstrated to have serious shortcomings. Methods used for their conjugation onto NPs are also highly sophisticated and there are no reports to date of clinical materials that were produced using this strategy. Because of the burgeoning application of ^{64}Cu-labeled NPs in translational research, alternative radiolabeling strategies have been developed and these have shown great potential for oncological applications (Hong et al. 2017; Zhao et al. 2014). Based on extensive research into nonradioactive Cu-PAMAM composites (Tang et al. 2017; Erturk et al. 2015; Ottaviani et al. 2013), we chose a commercially available nanoparticle, G5 PAMAM, to develop a ^{64}Cu-labeled NP system without the need for a chelator and demonstrated the feasibility of direct ^{64}Cu labeling of NPs.

G5 PAMAM, which balances the amount of internal cavities and economy, was selected as a template for ^{64}Cu labeling. To achieve better biocompatibility and Cu^{2+} complexation, maltose was conjugated to the surface amino groups of G5 PAMAM by a simple reductive amination reaction. Radioactive ^{64}Cu was produced using a commercially available module and confirmed to be free of other nuclide impurities using an HPGe detector. In the ^{64}Cu labeling experiments, different pH values, temperature, time, and amounts of G5-Mal were compared. When the pH value, temperature, and concentration of G5-Mal were 7, 25 °C, and 1 mg/mL, respectively, the labeling yield reached a plateau after 15 min of reaction (Fig. 4a). The time-yield assay lasted 35 min and neither further improvement in labeling yield nor degradation was observed over this time course. The correlation between pH value and labeling yield was then determined (Fig. 4b). The labeling yield

increased significantly as the pH value of the reaction solution became neutral, likely as a result of reduced protonation of amino groups. Under acidic conditions, some of the tertiary amine groups inside the G5-Mal_{88} are protonated and lose the ability to coordinate with $^{64}Cu^{2+}$ ions (Zhao et al. 1998; Ottaviani et al. 1997). When the pH value was higher and the reaction solution was basic, some flocculent precipitation emerged in the solution, which meant that the labeling yield could not be determined and included in the results. Next, the impact of temperature on labeling yield was evaluated. The labeling yield decreased with increasing temperature of the reaction system (Fig. 4c), largely because of the architecture of PAMAM. PAMAM is a globular tree-like polymer, which incorporates a large number of branches that are relatively fixed by hydrogen bonding interactions to form a spherical shape with interior cavities (Svenson and Tomalia 2005). As the temperature increases, the hydrogen bonding structure collapses and restriction between the branches is lost, causing the branches to become more flexible and able to fold back into the PAMAM interior (Aumanen et al. 2011). As a result, some of the internal cavities are occupied by the folded-back branches and the possibility of $^{64}Cu^{2+}$ coordination decreases, leading to a lower radiolabeling at high temperatures. Finally, the influence of amount of G5-Mal_{88} on labeling yield was examined. Different concentrations of G5-Mal (0.1, 0.2, 0.5, 1, 2, and 5 mg/mL) were reacted with $^{64}CuCl_2$ under the optimum conditions of time, pH value, and temperature. When the concentration of G5-Mal_{88} was < 1 mg/mL, the labeling yield was proportional to the amount of G5-Mal_{88} and reached 94.1% at 1 mg/mL. When the concentration of G5-Mal_{88} was increased beyond 1 mg/mL, the labeling yield remained at a steady level and showed no obvious improvement (Fig. 4d). Taking into account the effect of specific activity on PET imaging, 1 mg/mL was identified as the optimum concentration of G5-Mal_{88}. To summarize, the optimum conditions for $^{64}CuCl_2$ labeling of G5-Mal_{88} in this study were found to be reaction of $^{64}CuCl_2$ (10 μL) with G5-Mal_{88} (90 μL, 1 mg/mL) at 25 °C and pH 7 for 15 min. Once the optimum labeling parameters had been determined, the stability of G5-Mal_{88}-^{64}Cu was measured in PBS, EDTA solution, and mouse plasma. G5-Mal_{88}-^{64}Cu was found to be stable in PBS after 12-h incubation while some radioactive impurities were observed in EDTA solution and mouse plasma (Fig. 5). Since the EDTA is a strong chelating agent, the impurity was likely the ^{64}Cu-EDTA composition. In mouse serum, the impurities may be complexes comprised of $^{64}Cu^{2+}$ and plasma proteins. Because the G5 PAMAM was not completely blocked by maltose, there were still some gaps on the surface of G5 PAMAM which possibly allowed the internally coordinated ^{64}Cu ions to interact with proteins in plasma. Completely blocked PAMAM would decrease such impurities and this will be a topic for further research.

In order to evaluate the potential of direct $^{64}Cu^{2+}$-labeled NPs in vivo, the biodistribution of G5-Mal_{88}-^{64}Cu was measured in normal mice. High accumulation of G5-Mal_{88}-^{64}Cu in the liver and spleen (Fig. 6) indicated that G5-Mal_{88}-^{64}Cu displayed the bright characteristic of NPs, most of which are phagocytized by the reticuloendothelial system. Because of the small particle size, part of the G5-Mal_{88}-^{64}Cu was able to be excreted renally, resulting in a higher uptake in the kidney. Levels of G5-Mal_{88}-^{64}Cu in blood were a little high 30 min after injection (5.73 ± 0.71 ID%/g), which was largely attributed to degradation of G5-Mal_{88}-^{64}Cu in plasma. However, the clearance from blood was fast. The low blood and muscle biodistribution would not affect imaging and should lead to more accurate results in future applications. All other tissues showed much lower biodistributions of radioactivity. In the present study, G5 PAMAM was simply modified by attachment of maltose and further optimization should provide improved biodistribution data. Furthermore, there are a large number of dendrimers made up of different molecules that could be used for direct ^{64}Cu labeling. Here, we have introduced a simple idea for direct ^{64}Cu labeling of NPs and, building on this concept, optimum modification of different dendrimers should produce better results in future studies. This method is also likely to extend to other NPs with similar structures to PAMAM.

Conclusions

In brief, we have developed a novel, direct ^{64}Cu labeling method, based on G5 PAMAM, which does not require chelators. After a simple modification using maltose, G5-Mal_{88} was used as a template for direct ^{64}Cu labeling. The labeling time, pH value, temperature, and amount of G5-Mal_{88} were systematically varied to determine the best conditions for labeling. The optimum conditions for preparing ^{64}Cu-labeled G5-Mal_{88} were

found to be reaction of $^{64}CuCl_2$ (10 μL) with G5-Mal_{88} (90 μL, 1 mg/mL) at 25 °C and pH 7 for 15 min. The stability of G5-Mal_{88}-^{64}Cu and its biodistribution in mice were also evaluated. This study introduced a novel idea for chelator-free ^{64}Cu labeling of dendrimers (and other NPs with similar structures) and should facilitate the application of nanoparticles in biomedicine.

Funding information The research was financially supported by the National Natural Science Foundation of China (Grant No. 21401025) and Shanghai Engineering Research Center of Molecular Imaging Probes (Grant No. 14DZ2251400).

Compliance with ethical standards The animal study was approved by Fudan University Laboratory Animal Ethics Committee.

Conflict of interest The authors declare that they have no conflicts of interest.

References

Anderson CJ, Ferdani R (2009) Copper-64 radiopharmaceuticals for pet imaging of cancer: advances in preclinical and clinical research. Cancer Biother Radio 24:379–393

Aumanen J, Teobaldi G, Zerbetto F, Korppi-Tommola J (2011) The effect of temperature on the internal dynamics of dansylated POPAM dendrimers. RSC Adv 1:1778–1787. https://doi.org/10.1039/C1RA00625H

Balogh L, Valluzzi R, Laverdure KS, Gido SP, Hagnauer GL, Tomalia DA (1999) Formation of silver and gold dendrimer nanocomposites. J Nanopart Res 1:353–368. https://doi.org/10.1023/A:1010060404024

Bass LA, Wang M, Welch MJ, Anderson CJ (2000) In vivo transchelation of copper-64 from TETA-octreotide to superoxide dismutase in rat liver. Bioconjug Chem 11:527–532. https://doi.org/10.1021/bc9901671

Bose T, Latawiec D, Mondal PP, Mandal S (2014) Overview of nano-drugs characteristics for clinical application: the journey from the entry to the exit point. J Nanopart Res 16:2527. https://doi.org/10.1007/s11051-014-2527-7

Boswell CA, Sun X, Niu W, Weisman GR, Wong EH, Rheingold AL, Anderson CJ (2004) Comparative in vivo stability of copper-64-labeled cross-bridged and conventional tetraazamacrocyclic complexes. J Med Chem 47:1465–1474. https://doi.org/10.1021/jm030383m

Caminade AM, Ouali A, Laurent R, Majoral JP (2015) Phosphorus dendrimers as supports of transition metal catalysts. Inorg Chim Acta 431:3–20. https://doi.org/10.1016/j.ica.2014.10.035

Chen X (2011) Nanoplatform-based molecular imaging. John Wiley & Sons, Inc.

Cheng Z, Al Zaki A, Hui JZ, Muzykantov VR, Tsourkas A (2012) Multifunctional nanoparticles: cost versus benefit of adding targeting and imaging capabilities. Science 338:903–910. https://doi.org/10.1126/science.1226338

Colombo I, Overchuk M, Chen J, Reilly RM, Zheng G, Lheureux S (2017) Molecular imaging in drug development: update and challenges for radiolabeled antibodies and nanotechnology. Methods 130:23–35. https://doi.org/10.1016/j.ymeth.2017.07.018

Crooks RM, Zhao M, Sun L, Chechik V, Yeung LK (2001) Dendrimer-encapsulated metal nanoparticles: synthesis, characterization, and applications to catalysis. Accounts Chem Res 34:181–190. https://doi.org/10.1021/ar000110a

De Silva RA, Jain S, Lears KA, Chong H-S, Kang CS, Sun X et al (2012) Copper-64 radiolabeling and biological evaluation of bifunctional chelators for radiopharmaceutical development. Nucl Med Biol 39:1099–1104. https://doi.org/10.1016/j.nucmedbio.2012.05.009

Erturk AS, Gurbuz MU, Tulu M, Bozdogan AE (2015) Water-soluble TRIS-terminated PAMAM dendrimers: microwave-assisted synthesis, characterization and Cu(II) intradendrimer complexes. RSC Adv 5:60581–60595. https://doi.org/10.1039/c5ra11157a

Ficker M, Petersen JF, Gschneidtner T, Rasmussen A-L, Purdy T, Hansen JS, Hansen TH, Husted S, Moth Poulsen K, Olsson E, Christensen JB (2015) Being two is better than one-catalytic reductions with dendrimer encapsulated copper- and copper-cobalt-subnanoparticles. Chem Commun 51:9957–9960. https://doi.org/10.1039/C5CC00347D

Gajbhiye V, Ganesh N, Barve J, Jain NK (2013) Synthesis, characterization and targeting potential of zidovudine loaded sialic acid conjugated-mannosylated poly(propyleneimine) dendrimers. Eur J Pharm Sci 48:668–679. https://doi.org/10.1016/j.ejps.2012.12.027

Gawande MB, Goswami A, Felpin FX, Asefa T, Huang XX, Silva R, Zou X, Zboril R, Varma RS (2016) Cu and Cu-based nanoparticles: synthesis and applications in review catalysis. Chem Rev 116:3722–3811. https://doi.org/10.1021/acs.chemrev.5b00482

Heidel JD, Davis ME (2011) Clinical developments in nanotechnology for cancer therapy. Pharm Res 28:187–199. https://doi.org/10.1007/s11095-010-0178-7

Hong SH, Sun Y, Tang C, Cheng K, Zhang R, Fan Q, Xu L, Huang D, Zhao A, Cheng Z (2017) Chelator-free and biocompatible melanin nanoplatform with facile-loading gadolinium and copper-64 for bioimaging. Bioconjug Chem 28:1925–1930. https://doi.org/10.1021/acs.bioconjchem.7b00245

Kinnear C, Moore TL, Rodriguez-Lorenzo L, Rothen-Rutishauser B, Petri-Fink A (2017) Form follows function: nanoparticle shape and its implications for nanomedicine. Chem Rev 117:11476–11521. https://doi.org/10.1021/acs.chemrev.7b00194

Klajnert B, Appelhans D, Komber H, Morgner N, Schwarz S, Richter S, Brutschy B, Ionov M, Tonkikh A K, Bryszewska M, Voit B (2008) The influence of densely organized maltose shells on the biological properties of poly(propylene imine) dendrimers: new effects dependent on hydrogen bonding. Chem-Eur J 14:7030–7041. https://doi.org/10.1002/chem.200800342

Liu Y, Welch MJ (2012) Nanoparticles labeled with positron emitting nuclides: advantages, methods, and applications. Bioconjug Chem 23:671–682. https://doi.org/10.1021/bc200264c

Maity P, Yamazoe S, Tsukuda T (2013) Dendrimer-encapsulated copper cluster as a chemoselective and regenerable hydrogenation catalyst. ACS Catal 3:182–185. https://doi.org/10.1021/cs3007318

Murty BSSP, Raj B, Rath BB, Murday J (2013) Application of nanomaterials. In: Textbook of nanoscience and nanotechnology. Springer, Berlin, Heidelberg, pp 107–148

Nemanashi M, Meijboom R (2013) Synthesis and characterization of Cu, Ag and Au dendrimer-encapsulated nanoparticles and their application in the reduction of 4-nitrophenol to 4-aminophenol. J Colloid Interf Sci 389:260–267. https://doi.org/10.1016/j.jcis.2012.09.012

Ottaviani MF, Montalti F, Turro NJ, Tomalia DA (1997) Characterization of starburst dendrimers by the EPR technique. Copper(ii) ions binding full-generation dendrimers. J Phys Chem B 101:158–166. https://doi.org/10.1021/jp962857h

Ottaviani MF, Cangiotti M, Fattori A, Coppola C, Lucchi S, Ficker M, Petersen JF, Christensen JB (2013) Copper(II) complexes with 4-carbomethoxypyrrolidone functionalized PAMAM-dendrimers: an EPR study. J Phys Chem B 117:14163–14172. https://doi.org/10.1021/jp410307z

Padmanabhan P, Kumar A, Kumar S, Chaudhary RK, Gulyas B (2016) Nanoparticles in practice for molecular-imaging applications: an overview. Acta Biomater 41:1–16. https://doi.org/10.1016/j.actbio.2016.06.003

Pelaz B, Alexiou C, Alvarez-Puebla RA, Alves F, Andrews AM, Ashraf S, Balogh LP, Ballerini L, Bestetti A, Brendel C, Bosi S, Carril M, Chan WCW, Chen C, Chen X, Chen X, Cheng Z, Cui D, du J, Dullin C, Escudero A, Feliu N, Gao M, George M, Gogotsi Y, Grünweller A, Gu Z, Halas NJ, Hampp N, Hartmann RK, Hersam MC, Hunziker P, Jian J, Jiang X, Jungebluth P, Kadhiresan P, Kataoka K, Khademhosseini A, Kopeček J, Kotov NA, Krug HF, Lee DS, Lehr CM, Leong KW, Liang XJ, Ling Lim M, Liz-Marzán LM, Ma X, Macchiarini P, Meng H, Möhwald H, Mulvaney P, Nel AE, Nie S, Nordlander P, Okano T, Oliveira J, Park TH, Penner RM, Prato M, Puntes V, Rotello VM, Samarakoon A, Schaak RE, Shen Y, Sjöqvist S, Skirtach AG, Soliman MG, Stevens MM, Sung HW, Tang BZ, Tietze R, Udugama BN, VanEpps JS, Weil T, Weiss PS, Willner I, Wu Y, Yang L, Yue Z, Zhang Q, Zhang Q, Zhang XE, Zhao Y, Zhou X, Parak WJ (2017) Diverse applications of nanomedicine. ACS Nano 11:2313–2381. https://doi.org/10.1021/acsnano.6b06040

Rosenblum LT, Kosaka N, Mitsunaga M, Choyke PL, Kobayashi H (2010) In vivo molecular imaging using nanomaterials: general in vivo characteristics of nano-sized reagents and applications for cancer diagnosis. Mol Membr Biol 27:274–285. https://doi.org/10.3109/09687688.2010.481640

Shi J, Kantoff PW, Wooster R, Farokhzad OC (2016) Cancer nanomedicine: progress, challenges and opportunities. Nat Rev Cancer 17:20–37. https://doi.org/10.1038/nrc.2016.108

Smith BR, Gambhir SS (2017) Nanomaterials for in vivo imaging. Chem Rev 117:901–986. https://doi.org/10.1021/acs.chemrev.6b00073

Svenson S, Tomalia DA (2005) Dendrimers in biomedical applications—reflections on the field. Adv Drug Deliver Rev 57:2106–2129. https://doi.org/10.1016/j.addr.2005.09.018

Taghavi Pourianazar N, Mutlu P, Gunduz U (2014) Bioapplications of poly(amidoamine) (PAMAM) dendrimers in nanomedicine. J Nanopart Res 16:2342. https://doi.org/10.1007/s11051-014-2342-1

Tang YH, Cangiotti M, Kao CL, Ottaviani MF (2017) EPR characterization of copper(ii) complexes of PAMAM-py dendrimers for biocatalysis in the absence and presence of reducing agents and a spin trap. J Phys Chem B 121:10498–10507. https://doi.org/10.1021/acs.jpcb.7b09464

Tiwari A, Mishra AK, Kobayashi H, Turner APF (2012) Intelligent nanomaterials: processes, properties, and applications. John Wiley & Sons, Inc.

Wadas TJ, Anderson CJ (2007) Radiolabeling of TETA- and CB-TE2A-conjugated peptides with copper-64. Nat Protoc 1:3062–3068. https://doi.org/10.1038/nprot.2006.431

Wadas TJ, Wong EH, Weisman GR, Anderson CJ (2010) Coordinating radiometals of copper, gallium, indium, yttrium, and zirconium for PET and SPECT imaging of disease. Chem Rev 110:2858–2902. https://doi.org/10.1021/cr900325h

Wang Y, Liu Y, Luehmann H, Xia X, Brown P, Jarreau C, Welch M, Xia Y (2012) Evaluating the pharmacokinetics and in vivo cancer targeting capability of au nanocages by positron emission tomography imaging. ACS Nano 6:5880–5888. https://doi.org/10.1021/nn300464r

Wang S, Cazelles R, Liao W-C, Vázquez-González M, Zoabi A, Abu-Reziq R, Willner I (2017) Mimicking horseradish peroxidase and nadh peroxidase by heterogeneous Cu^{2+}-modified graphene oxide nanoparticles. Nano Lett 17:2043–2048. https://doi.org/10.1021/acs.nanolett.7b00093

Xing Y, Zhao JH, Conti PS, Chen K (2014) Radiolabeled nanoparticles for multimodality tumor imaging. Theranostics 4:290–306. https://doi.org/10.7150/thno.7341

Zhang Y, Xu X, Wang L, Lin J, Zhu Y, Guo Z, Sun Y, Wang H, Zhao Y, Tai R, Yu X, Fan C, Huang Q (2013) Dendrimer-folate-copper conjugates as bioprobes for synchrotron X-ray fluorescence imaging. Chem Commun 49:10388–10390. https://doi.org/10.1039/C3CC46057F

Zhao M, Sun L, Crooks RM (1998) Preparation of Cu nanoclusters within dendrimer templates. J Am Chem Soc 120:4877–4878. https://doi.org/10.1021/ja980438n

Zhao FG, Li WS (2011) Dendrimer/inorganic nanomaterial composites: tailoring preparation, properties, functions, and applications of inorganic nanomaterials with dendritic architectures. Sci China Chem 54:286–301. https://doi.org/10.1007/s11426-010-4205-7

Zhao Y, Sultan D, Detering L, Cho S, Sun G, Pierce R, Wooley KL, Liu Y (2014) Copper-64-alloyed gold nanoparticles for cancer imaging: improved radiolabel stability and diagnostic accuracy. Angew Chem Int Edit 53:156–159. https://doi.org/10.1002/anie.201308494